Available online at www.sciencedirect.com

ScienceDirect

Mendeleev Commun., 2024, **34**, 221–223

Mendeleev Communications

Methane dry reforming: influence of the SiO_2 and Al_2O_3 supports on the catalytic properties of Ni catalysts

Alexander L. Kustov,*[a,b] Timur R. Aymaletdinov,[a] Anastasiya A. Shesterkina,[a,b] Konstantin B. Kalmykov,[a] Petr V. Pribytkov,[a,b] Igor V. Mishin,[b] Sergey F. Dunaev[a] and Leonid M. Kustov[a,b]

[a] *Department of Chemistry, M. V. Lomonosov Moscow State University, 119991 Moscow, Russian Federation. E-mail: kyst@list.ru*

[b] *N. D. Zelinsky Institute of Organic Chemistry, Russian Academy of Sciences, 119991 Moscow, Russian Federation*

DOI: 10.1016/j.mencom.2024.02.020

The effect of the support nature (SiO_2, Al_2O_3, SiO_2–Al_2O_3) on the catalytic performance of Ni-based catalysts prepared by the incipient wetness method was explored in the dry reforming of methane reaction, and the catalysts were characterized by TG-DTA, SEM-EDX, XRD and UV-VIS methods. The results demonstrate that NiO supported on SiO_2-modified Al_2O_3 exhibits superior catalytic performance in methane dry reforming in the temperature range of 650–700 °C.

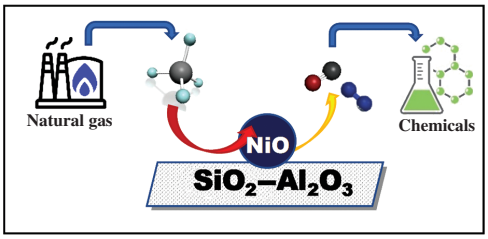

Keywords: dry reforming, methane, nickel catalysts, supported catalyst, aluminium oxide.

Dry reforming of methane (DRM) with carbon dioxide to produce synthesis gas has attracted much attention from both environmental and industrial aspects.[1] The environmental impact of the DRM reaction is related to utilization and consumption of two abundant greenhouse gases (CH_4 and CO_2).[2–4] Syngas is one of the most important intermediate products in chemical industry and can be used for the Fischer–Tropsch or methanol synthesis to produce high-value chemicals.[5,6] The main disadvantage of the DRM reaction is the use of high temperatures, which results in sintering of active metal particles, coke formation and loss of activity of catalysts.[7–9] Noble metal catalysts such as Ru, Rh, Pd, Ir and Pt are the most catalytically active and stable ones in DRM, but their high cost makes the process economically impractical.[10–12] Currently, nickel-containing catalysts supported on Al_2O_3, SiO_2, ZrO_2, TiO_2, MgO and zeolite ZSM-5 are a good and cheap alternative due to their similar or even higher activity.[13–18] The catalyst support plays a decisive role in supported metal catalysts, since the catalytic properties depend not only on the nature of the active metal, but also on its dispersion and interaction with the support.[19]

The aim of our work was to investigate the effect of the support such as SiO_2 with different specific surface areas (SiO_2-LS with a low specific surface area and SiO_2-HS with a high specific surface area), Al_2O_3 and SiO_2 modified with Al_2O_3 (SiO_2–Al_2O_3) on the catalytic properties of Ni-containing catalysts in the DRM reaction. Herein, the synthesis of the supported Ni-containing catalysts is described.† The prepared supported Ni catalysts were characterized by TG-DTA, SEM-EDX, XRD and UV-VIS spectroscopy. The TG-DTA studies revealed the conditions of decomposition of the supported precursor. The thermogravimetric (TG) and corresponding differential thermogravimetric (DTG) and differential thermal analysis (DTA) curves of the dried samples after impregnation on different supports are shown in Figures S1–S4 (see Online Supplementary Materials). Decomposition of supported phases proceeds stepwise and depends on the support. Two major mass loss regions were observed on the TG curve of all nickel samples: (*1*) a slow decrease in the weight at 80–220 °C with heat absorption and (*2*) rapid weight reduction with heat absorption at 240–350 °C. The loss of the weight during heat consumption at a temperature up to 220 °C is most likely due to the smooth release of structural water. The second endothermic weight loss may be assigned to the decomposition of nickel nitrate. The

† Supported 10 wt% Ni catalysts were synthesized by the incipient wetness impregnation of the pre-evacuated supports γ-Al_2O_3, SiO_2 with the different specific surface areas (SiO_2-HS, SiO_2-LS), SiO_2–Al_2O_3 with an aqueous solution of metal precursors, $Ni(NO_3)_2 \cdot 6H_2O$, with a required concentration, followed by drying at 110 °C for 12 h in a drying oven. Then the dry samples were subjected to thermal treatment in air at 800 °C for 24 h. Commercial γ-Al_2O_3 (S_{BET} = 260 m^2 g^{-1}; V_{pore} = 0.83 cm^3 g^{-1}; Saint-Gobain), SiO_2-LS (S_{BET} = 108 m^2 g^{-1}; V_{pore} = 1.05 cm^3 g^{-1}, KSKG trade mark, Chimmed), SiO_2-HS (S_{BET} = 260 m^2 g^{-1}; V_{pore} = 1.01 cm^3 g^{-1}, Saint-Gobain) and SiO_2–Al_2O_3 (SiO_2 modified with Al_2O_3, 75–95% SiO_2, 5–25% Al_2O_3, S_{BET} = 400 m^2 g^{-1}; V_{pore} = 0.6 cm^3 g^{-1}; Saint-Gobain) were used as supports for Ni-containing nanoparticles. The synthesized materials were marked as Ni/X, where X is the support.

The DRM reaction was performed in a tubular fixed-bed continuous-flow reactor that consisted of a quartz tube with an inner diameter of 8 mm under atmospheric pressure. The calcined samples were examined in the DRM reaction without an additional activation step. The loading (0.5 g) of a shaped catalyst (0.25–0.5 mm) was mixed with quartz so that the total volume was 2 cm^3 and the sample was placed at the center of the reactor. Before the catalytic experiment, the reactor was purged with argon. The reaction was carried out in the temperature range of 550–700 °C with a step of 25 °C, the molar ratio of CO_2/CH_4 was equal to 1.2. The gas composition of reactants and products were analyzed on-line using a Crystal 5000 gas chromatograph equipped with four columns for each gas, TCD detector and flame ionization detector.

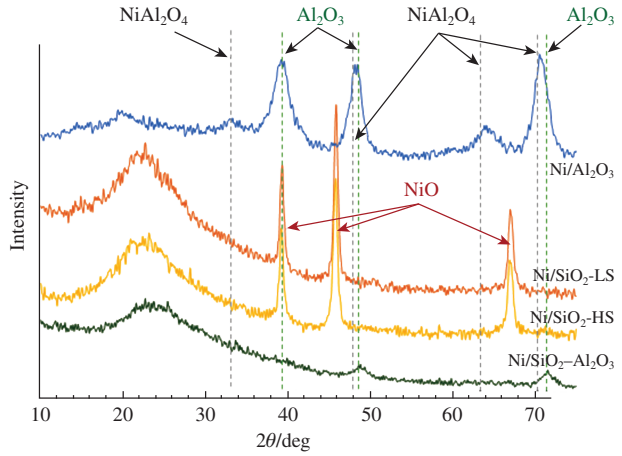

Figure 1 XRD patterns of Ni catalysts.

maximum total weight loss was 23% for the sample supported on SiO_2–Al_2O_3, while it did not exceed 19% for catalysts on other supports.

The XRD pattern of the calcined nickel catalysts supported on SiO_2 and SiO_2–Al_2O_3 (Figure 1) has shown the peak positions at 37.3, 43.3, and 62.8°, which manifests signals for cubic nickel oxide NiO (JCPDS # 47–1049).[20] The diffraction patterns of the calcined samples Ni/Al_2O_3 and Ni/SiO_2–Al_2O_3 contain reflections at 2θ of 37.6, 45.8, and 66.8°, which can be attributed to the (311), (222), and (400) faces of γ-Al_2O_3 (ICDD-PDF map no. 04-088),[21] however, the cubic structure of the $NiAl_2O_4$ phase (peaks positions at 37.0, 44.5, 59.6 and 65.5°)[22] was found only in the Ni/Al_2O_3 catalyst.

The results of the UV-VIS study of the synthesized catalysts are shown in Figure 2. Nickel nanoparticles supported on SiO_2 and SiO_2–Al_2O_3 demonstrate bands in the range of 200–800 nm characteristic of the NiO phase, two intense bands in the UV

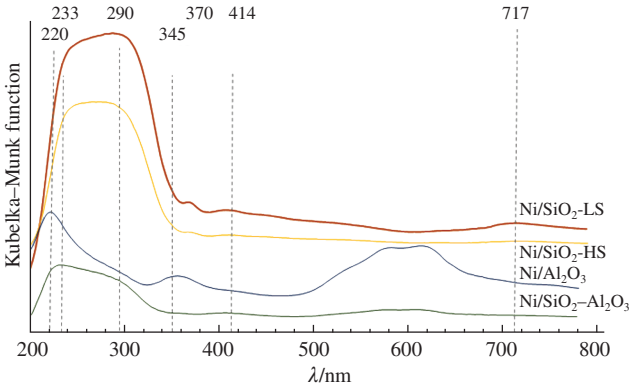

Figure 2 UV-VIS diffuse reflectance spectra of the calcined supported Ni catalysts.

Table 1 Distribution of the main elements on the surface of catalysts based on the SEM-EDX data.

Catalyst	Element content (wt%)			
	Ni[a]	O	Si	Al
Ni/Al_2O_3	11.38	47.33	–	41.29
Ni/SiO_2-HS	11.71	46.53	42.76	–
Ni/SiO_2–Al_2O_3	14.69	46.87	26.99	11.45
Ni/SiO_2-LS	9.45	51.15	38.24	0.15

[a] Set content of Ni during the synthesis of all the catalysts was 10.00%.

region of 220–270 and 280–310 nm can be attributed to the charge transfer O^{2-}→Ni^{2+}, and the other four bands in the visible region correspond to d–d transitions.[23] Alumina-based nickel catalysts exhibit bands in the ultraviolet region at 220 and 345 nm responsible for the charge transfer of O^{2-}→Ni^{2+}. The bands in the range of 380–720 nm belong to the d–d transitions of the nickel atom characteristic of $NiAl_2O_4$ particles, which is consistent with the XRD data for this sample.[24]

SEM microphotographs of all the samples and the detailed composition determined by the EDX method can be found in Online Supplementary Materials, Figures S5–S8. The obtained images show that nickel nanoparticles in all supported catalysts are uniformly distributed over the surface of all supports. However, it can be noticed that the particles in the samples deposited on the supports SiO_2 and SiO_2–Al_2O_3 have an average size of 0.2 to 0.5 μm, while larger particles up to 2 μm are observed on Al_2O_3. The generalized results of the EDX studies are presented in Table 1. Based on the results obtained, it can be seen that the theoretical and experimental ratios of the active element Ni on the SiO_2 and Al_2O_3 supports are preserved. For the supported samples on SiO_2–Al_2O_3, overestimated values of the mass content of nickel on the surface relative to the specified content at the stage of preparation of catalysts were obtained (see Table 1). This is probably achieved by depositing metal precursors preferably at the outer surface of the samples.

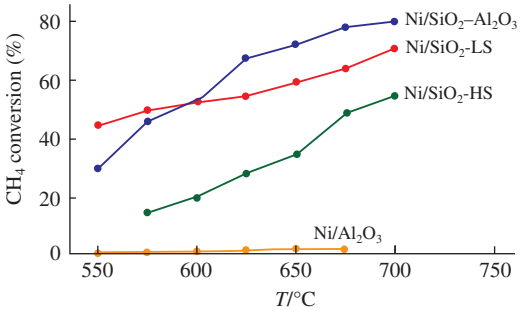

Figure 3 The temperature dependence of the methane conversion on the supported Ni catalysts.

Table 2 Catalytic properties of nickel-containing catalysts in methane dry reforming.

Entry	Catalyst	Reaction conditions[a]	Conversion (%)	Selectivity (%)	Ref.
1	$Ni/(Nd_2O_3,CaO)$	700 °C, CH_4/CO_2 = 1 : 1	80	80	1
2	$Ni/La_{0.8}Mg_{0.2}AlO_{2.9}$	1 bar; 700 °C, CH_4/CO_2/Ar = 1 : 1 : 2 WHSV = 96 000 ml h^{-1} g^{-1}	75	no data available	3
3	Ni/SiO_2	800 °C, 1 bar, CH_4/CO_2 = 1 : 1 WHSV = 20 000 ml h^{-1} g^{-1}	70	no data available	4
4	Ni/Al_2O_3	625 °C; $CH_4/CO_2/N_2$ = 1 : 1 : 5 GHSV = 42 000 ml h^{-1} g^{-1}	60	100	25
5	Ni/Al_2O_3–ZrO_2	800 °C, $CH_4/CO_2/N_2$ = 2 : 2 : 1 WHSV = 11 160 ml h^{-1} g^{-1}	83	100	26
6	Ni/SiO_2–Al_2O_3	700 °C, CO_2/CH_4 = 1.2	81	100	This work

[a] Unit g^{-1} in the WHSV/GHSV parameters stands for gram of the catalyst.

The prepared catalysts were investigated in DRM in the temperature range of 550–700 °C at an atmospheric pressure. The activity test results are shown in Figure 3. It was revealed that the CH_4 conversion increased gradually with increasing temperature, which was caused by the strong endothermic reaction of methane reforming. Catalysts with a similar nickel content supported onto various carriers showed significant differences in the catalytic characteristics of the DRM reaction, which illustrated the significant effect of the nature of the support on the activity of the catalyst. Nickel nanoparticles supported on Al_2O_3 were not active, the reason for this was the formation of the $NiAl_2O_4$ phase at the calcination stage during the synthesis of the sample. When using SiO_2 instead of Al_2O_3 as a support of the nickel catalyst, the CH_4 conversion greatly increased. However, the use of SiO_2-LS with a smaller specific surface area led to almost twofold increase in the conversion over the entire temperature range. The $Ni/SiO_2–Al_2O_3$ catalyst exhibited the optimal catalytic performance among the four catalysts, and the CH_4 conversion for this catalyst at temperatures of 650–700 °C was above 80%. This catalyst was active for 40 h at a temperature of 700 °C (Figure S9). The product selectivity for all catalysts was 100%.

Table 2 presents the results of methane dry reforming on nickel-containing catalysts obtained in this work compared to the previously described ones. It can be seen that in order to reach a high conversion of methane, high reaction temperatures are required.

This work was supported by the Ministry of Science and Higher Education of the Russian Federation (grant no. 075-15-2023-585).

Online Supplementary Materials

Supplementary data associated with this article can be found in the online version at doi: 10.1016/j.mencom.2024.02.020.

References

1 S. A. Malyshev, O. A. Shlyakhtin, A. S. Loktev, G. N. Mazo, G. M. Timofeev, I. E. Mukhin, R. D. Svetogorov, I. V. Roslyakov and A. G. Dedov, *Materials*, 2022, **15**, 7265.
2 B. Abdullah, N. A. Abd Ghani and D. N. N. Vo, *J. Cleaner Prod*., 2017, **162**, 170.
3 X. Bai, G. Xie, Y. Guo, L. Tian, H. M. El-Hosainy, A. E. Awadallah, S. Ji and Z. Wang, *Catal. Today*, 2021, **368**, 78.
4 W. Kong, Y. Fu, L. Shi, S. Li, E. Vovk, X. Zhou, R. Si, B. Pan, C. Yuan, S. Li, F. Cai, H. Zhu, J. Zhang, Y. Yang and Y. Sun, *Appl. Catal., B*, 2021, **285**, 119837.
5 X. Wu, L. Xu, M. Chen, C. Lv, X. Wen, Y. Cui, C. Wu, B. Yang, Z. Mao and X. Hu, *Front. Chem.*, 2020, **8**, 581923.
6 K. Lorber, J. Zavašnik, J. Sancho-Parramon, M. Bubaš, M. Mazaj and P. Djinović, *Appl. Catal., B*, 2022, **301**, 120745.
7 W.-J. Jang, J.-O. Shim, H.-M. Kim, S.-Y. Yoo and H.-S. Roh, *Catal. Today*, 2019, **324**, 15.
8 N. A. K. Aramouni, J. G. Touma, B. A. Tarboush, J. Zeaiter and M. N. Ahmad, *Renewable Sustainable Energy Rev*., 2018, **82**, 2570.
9 S. Arora and R. Prasad, *RSC Adv*., 2016, **6**, 108668.
10 Á. A. Moreno, T. R. Raina, S. Ivanova, A.-C. Roger, M. Á. Centeno and J. A. Odriozola, *Front. Chem.*, 2021, **9**, 694976.
11 J. Niu, Y. Wang, S. E. Liland, S. K. Regli, J. Yang, K. R. Rout, J. Luo, M. Rønning, J. Ran and D. Chen, *ACS Catal*., 2021, **11**, 2398.
12 Z. Qin, J. Chen and X. Xie, *Environ. Chem. Lett*., 2020, **18**, 997.
13 S. Dekkar, S. Tezkratt, D. Sellam, K. Ikkour, K. Parkhomenko, A. Martinez-Martin and A. C. Roger, *Catal. Lett*., 2020, **150**, 2180.
14 C. Wang, H. Wu, X. Jie, X. Zhang, Y. Zhao, B. Yao and T. Xiao, *ACS Appl. Mater. Interfaces*, 2021, **13**, 3169.
15 C. Chen, W. Wan, Q. Ren, R. Ye, N. Nie, Z. Liu, L. Zhan and J. Xiao, *Front. Chem.*, 2022, **10**, 993691.
16 P. Hongmanorom, J. Ashok, G. Zhang, Z. Bian, M. H. Wai, Y. Zeng, S. Xi, A. Borgna and S. Kawi, *Appl. Catal., B*, 2021, **282**, 119564.
17 P. Frontera, A. Macario, A. Aloise, P. L. Antonucci, G. Giordano and J. B. Nagy, *Catal. Today*, 2013, **218**, 18.
18 B. Sarkar, R. Goyal, C. Pendem, T. Sasaki and R. Bal, *J. Mol. Catal. A: Chem*., 2016, **424**, 17.
19 I. V. Zagaynov, A. S. Loktev, I. E. Mukhin, A. A. Konovalov and A. G. Dedov, *Mendeleev Commun*., 2022, **32**, 129.
20 A. A. Shesterkina, K. V. Vikanova, V. S. Zhuravleva, A. L. Kustov, N. A. Davshan, I. V. Mishin, A. A. Strekalova and L. M. Kustov, *Mol. Catal.*, 2023, **547**, 113341.
21 E. V. Golubina, E. S. Lokteva, N. E. Kavalerskaya and K. I. Maslakov, *Kinet. Catal*., 2020, **61**, 444 (*Kinet. Katal.*, 2020, **61**, 410).
22 L. Landa, A. Remiro, J. Valecillos, B. Valle, J. Bilbao and A. G. Gayubo, *Fuel*, 2022, **321**, 124009.
23 B. Li, X. Lin, Y. Luo, X. Yuan and X. Wang, *Fuel Process. Technol*., 2018, **176**, 153.
24 Z. Boukha, C. Jiménez-González, B. de Rivas, J. R. González-Velasco, J. I. Gutiérrez-Ortiz and R. López-Fonseca, *Appl. Catal., B*, 2014, **158–159**, 190.
25 A. Valentini, N. L. V. Carreno, L. F. D. Probst, P. N. Lisboa-Filho, W. H. Schreiner, E. R. Leite and E. Lingo, *Appl. Catal., A*, 2003, **255**, 211.
26 H. Li and J. Wang, *Chem. Eng. Sci*., 2004, **59**, 4861.

Received: 7th November 2023; Com. 23/7295